Earth and Planetary Science Letters, 84 (1987) 1–14
Elsevier Science Publishers B.V., Amsterdam – Printed in The Netherlands

[1]

Diverse eucritic pebbles in the Vaca Muerta mesosiderite

Alan E. Rubin and Eric A. Jerde

Institute of Geophysics and Planetary Physics, University of California, Los Angeles, CA 90024 (U.S.A.)

Received August 6, 1986; revised version accepted March 11, 1987

Seven 5-cm basaltic pebbles from the Vaca Muerta mesosiderite were analyzed by instrumental neutron activation analysis and electron microprobe. Three additional pebbles were only examined petrographically. Two pebbles are impact-melt breccias, four are similar texturally to main-group eucrites or some clasts in polymict eucrites, three are similar to cumulate eucrites and one is a fragmental breccia, similar to certain polymict eucrites. Cumulate pebbles have extremely low REE concentrations and high Eu/Sm ratios, reflecting the virtual absence of intercumulus liquid. Siderophile interelement ratios in the pebbles are similar to those in Vaca Muerta metal except for anomalously low Ir. Higher silica and merrillite in the pebbles relative to eucrites may reflect reduction of FeO in the silicates by P from mesosiderite metal. Pebbles were annealed following incorporation into the Vaca Muerta host; impacts were the dominant heat source. The occurrence of 20% impact-melt breccias among the pebbles and ~ 35–40% melt breccias among mesosiderite whole-rocks indicate that mesosiderites were more extensively impact-melted than howardites. We suggest three alternative models to account for this: (1) mesosiderites were derived from a separate parent body that experienced a higher meteoroid fluence than the basaltic achondrite parent body, (2) the low-velocity accretion of large metallic core fragments from disrupted differentiated asteroids led to metal enrichment of a few regions of the regolith and heat retention in these (mesosideritic) regions, and (3) mesosideritic regolith regions were less likely to be reduced to fine particles by extensive shock than howarditic regions.

1. Introduction

Mesosiderites are meteorite regolith breccias consisting of roughly equal amounts of metallic Fe-Ni and mafic silicates. The silicates consist of pyroxenitic and basaltic fragments as well as isolated grains of orthopyroxene, pigeonite, plagioclase and olivine. Although many basaltic fragments are similar to main-group and cumulate eucrites, some highly recrystallized and impact-melted fragments exhibit textures unknown among eucrites.

Previous workers [1–3] divided the mesosiderites into four types (1–4) reflecting increasing degrees of recrystallization. Type 1 mesosiderites are the least recrystallized and contain fine-grained matrices and angular mineral and rock fragments; type 4 mesosiderites contain a melt matrix and are probably impact-melt breccias [2].

Specimens of the Vaca Muerta subgroup 1A mesosiderite were found near Taltal, Atacama, Chile in 1861; several large masses ranging up to 25 kg were eventually recovered. Recent field work by Robert Haag resulted in the discovery of 10 basaltic pebbles that had been liberated from the metal matrix of Vaca Muerta by terrestrial weathering. Our analyses of these pebbles constitutes the first petrographic-compositional study of large discrete rocks within an individual mesosiderite.

2. Analytical procedures

Two adjacent 2-mm thick slabs were cut from pebbles 1–7. One set of slabs was used for the preparation of thin sections, the other for instrumental neutron activation analysis (INAA). Replicate samples from the centers of pebbles 6 and 7 were also analyzed. Pebbles 8–10 were only examined petrographically.

Minerals were analyzed with the UCLA Cameca "Camebax-microbeam" and automated ARL electron microprobes, using crystal spectrometers and following standard correction procedures [4]. Minerals were point-counted on the ARL microprobe; mineral vol.% was converted into wt.%

0012-821X/87/$03.50

TABLE 1

Bulk compositions of Vaca Muerta pebbles. Elements determined by instrumental neutron activation analysis; Mg, Al, Si, Ca, Ti and FeO determined by electron microprobe analysis of fused beads

Pebble	Mass (mg)	Na (mg/g)	Mg (mg/g)	Al (mg/g)	Si (mg/g)	K (μg/g)	Ca (mg/g)	Sc (μg/g)
1	333	2.91	39.0	71.3	226	198	74.6	26.2
2	340	2.72	40.9	64.0	230	155	72.9	28.4
3	370	2.69	41.1	66.2	225	148	73.9	26.4
4	320	2.65	44.4	57.1	225	149	69.6	28.6
5	334	2.80	37.8	73.6	230	159	75.8	26.4
6 [a]	334/363	2.01	53.3	81.0	224	99	71.5	25.8
7 [a]	335/361	2.48	47.4	74.4	232	117	74.2	26.1
Relative error(%)		< 2	< 2	< 2	< 2	10–15	2	< 2
H [b]		5.74	142	11.5	171	819	11.9	7.5

Pebble	Ti (mg/g)	Cr (mg/g)	Mn (mg/g)	Fe (mg/g)	FeO (mg/g)	Co (μg/g)	Ni (mg/g)	Ga (μg/g)
1	3.48	2.18	3.91	138	182	29.7	0.59	1.44
2	4.80	2.17	4.05	134	180	22.2	0.62	1.46
3	4.02	2.02	3.85	136	187	35.5	1.11	1.59
4	4.98	2.81	4.05	148	204	62.6	1.69	1.66
5	2.46	1.88	3.82	127	170	15.5	0.29	1.54
6 [a]	0.45	2.70	3.89	123	154	44.7	1.20	1.60
7 [a]	0.69	2.78	3.82	126	162	38.6	1.16	1.41
Relative error(%)	< 2	< 2	2	< 2	< 2	< 2	2–3	10–15
H [b]	0.62	3.40	2.24	276	88.7	810	18.0	5.77

Pebble	La (μg/g)	Ce (μg/g)	Nd (μg/g)	Sm (μg/g)	Eu (μg/g)	Tb (μg/g)	Ho (μg/g)	Yb (μg/g)
1	2.05	4.50	3.19	1.07	0.62	0.27	0.42 [d]	1.38
2	2.41	5.36	3.93	1.43	0.61	0.39	0.53	1.83
3	2.01	4.51	3.69	1.16	0.54	0.30	0.40	1.43
4	2.02	4.87	3.66	1.19	0.58	0.30	0.44 [d]	1.54
5	0.72 [c]	2.03	1.41 [c]	0.55	0.53	0.17	0.27 [d]	1.05
6 [a]	< 0.04	< 1.3	< 1.6	0.004 [d]	0.34	< 0.03	< 0.11	0.12 [d]
7 [a]	< 0.06	< 1.2	< 1.4	0.010 [d]	0.38	< 0.07	< 0.33	0.16 [d]
Relative error(%)	2–4	4–6	6–8	2–4	2	4–6	3	2
H [b]	0.33	0.88	0.60	0.181	0.069	0.047	0.07	0.20

Pebble	Lu (μg/g)	Hf (μg/g)	Ta (μg/g)	Ir (ng/g)	Au (ng/g)	Th (μg/g)	*mg**
1	0.22	0.92	0.09	< 4.6	10.7	0.27	0.387
2	0.27	1.03	0.14	2.0	4.51 [c]	0.24	0.402
3	0.22	0.93	0.13	< 4.5	9.61	0.22	0.394
4	0.24	0.94	0.12	4.4 [d]	19.0	0.26	0.392
5	0.16 [c]	0.50	0.05 [c]	< 4.5	5.35 [c]	0.25 [c]	0.396
6 [a]	0.024 [c]	< 0.21	< 0.03	< 4.7	9.05	< 0.16	0.506
7 [a]	0.034 [c]	< 0.19	< 0.03	2.0	6.51	< 0.15	0.464
Relative error(%)	2	2–4	4–6	4–6	4–6	6–8	
H [b]	0.034	0.18	0.029	740	230	0.041	0.825

*mg** = molar MgO/(MgO + FeO) determined from fused beads.

[a] Mean of two analyses.

[b] H-chondrite data used for normalization (compiled from published and unpublished sources).

[c] Relative errors 2–5× higher for this sample.

[d] Relative errors 5–10× higher for this sample.

using estimated mineral densities.

INAA irradiations were for 4 hours at the University of California, Irvine, with a neutron flux of $\sim 1.8 \times 10^{12}$ neutrons cm^{-2} s^{-1}. A series of four counts was made over the next four weeks using large volume cylindrical and low-energy planar Ge detectors. INAA data (Table 1) were reduced using the SPECTRA program [5,6].

Fused beads were prepared by heating 20 mg aliquots of the remaining powdered samples on Mo foil under an Ar atmosphere in a strip-heater. Concentrations of SiO_2, CaO, TiO_2, FeO, MgO and Al_2O_3 were determined in the glass beads with the ARL electron microprobe. Relative to the INAA data, the concentrations of Fe determined in the fused beads are high by 2–7%. This discrepancy is approximately within analytical uncertainty; replicate INAA analyses often vary in Fe by ~ 5%.

3. Results

3.1. Petrography and mineralogy

Although roughly uniform in size (~ 5 cm), the pebbles range in shape from subrounded to angular. All are basaltic and consist of major pyroxene, plagioclase and silica (tridymite or cristobalite) and accessory troilite, metallic Fe-Ni, ilmenite, merrillite and chromite, titanian chromite and chromian ülvospinel (solid solution series members here referred to simply as chromite) (Table 2). Many merrillite and silica grains occur adjacent to grains of metallic Fe-Ni and troilite.

Most of the pyroxene grains in the pebbles are inverted pigeonite, consisting of orthopyroxene with one or two sets of augite exsolution lamellae. Many pyroxene grains contain a few thick lamellae (generally 10–50 μm wide) parallel to (001); far more numerous are the fine, closely-spaced lamellae parallel to (100). Many pyroxene grains exhibit simple twinning; none of the grains is compositionally zoned. Pyroxene compositions (Table 3) are plotted in Fig. 1. Individual analyses lie along trends extending from the orthopyroxene to the augite fields subparallel to the Fs-Hd boundary of the pyroxene quadrilateral.

Plagioclase exhibits both polysynthetic and Carlsbad twinning; rare grains exhibit sector zoning. Many large grains enclose small inclusions of silica; some enclose small inclusions of pigeonite. In some cases, these inclusions seem to be preferentially oriented subparallel to the boundaries of the enclosing crystal. Such inclusions may be related to plagioclase-clouding in eucrites [7]. Plagioclase compositions (Ab 6–10) (Table 3) are all in the anorthite range; none of the grains is compositionally zoned.

Although similar in mineralogy, the pebbles have distinct textures. Each pebble thus represents a discrete rock type present in the Vaca Muerta regolith.

Pebble 1 has a subophitic texture (Fig. 2a); the average grain size is ~ 800 μm. One fine-grained (100–200 μm) region (~ 10 mm^2 in cross-sectional area) (Fig. 2b) contains more silica (7 vs. 4 wt.%) and somewhat less plagioclase (31 vs. 34 wt.%) than the rest of the pebble. A few regions of pebble 1 contain tabular plagioclase crystals and

TABLE 2

Mineral abundances (wt.%) in Vaca Muerta pebbles

	1	2	3	4	5	6	7	8	9	10
Plagioclase	34.1	35.1	37.9	36.6	35.3	44.9	36.9	37.6	31.9	36.9
Pigeonite	60.6	55.4	55.6	52.5	56.7	45.8	54.5	55.6	63.2	56.0
Silica	4.0	6.1	4.8	6.0	6.8	5.4	5.2	5.7	2.7	4.5
Chromite	0.8	0.3	< 0.3	< 0.3	0.7	< 0.3	0.6	< 0.3	0.9	0.3
Ilmenite	0.5	1.5	0.3	0.6	< 0.3	< 0.3	< 0.3	< 0.3	0.5	< 0.3
Merrillite	< 0.2	0.2	0.2	< 0.2	< 0.2	0.2	0.6	< 0.2	< 0.2	0.2
Troilite	< 0.3	0.9	1.2	2.8	0.6	3.1	2.2	1.1	0.8	1.3
Metallic Fe-Ni	< 0.5	< 0.5	< 0.5	1.5	< 0.5	0.5	< 0.5	< 0.5	< 0.5	0.9
Total	100.0	99.5	100.0	100.0	100.1	99.9	100.0	100.0	100.0	100.1
Points counted	636	527	522	524	547	528	541	524	555	560
Area (mm^2)	57	274	293	377	220	229	385	173	120	445

TABLE 3

Mineral compositions (wt.%) in Vaca Muerta pebbles.

	1	2	3	4	5	6	7
Pyroxene							
Number of grains	15	15	14	16	15	15	15
SiO_2	50.5	50.7	50.7	50.5	50.5	52.4	51.7
TiO_2	0.49	0.45	0.38	0.47	0.58	0.12	0.18
Al_2O_3	0.64	0.45	0.37	0.59	0.79	0.43	0.36
Cr_2O_3	0.23	0.15	0.13	0.24	0.24	0.24	0.20
FeO	27.8	29.3	30.5	28.2	26.4	25.7	27.1
MnO	1.0	1.0	1.0	1.0	1.0	1.0	1.0
MgO	12.2	12.6	12.4	12.4	12.0	16.6	15.6
CaO	7.7	6.2	5.2	7.5	9.2	4.3	4.3
Na_2O	< 0.02	< 0.02	< 0.02	< 0.02	0.03	0.02	< 0.02
Total	100.5	100.8	100.7	100.9	100.7	100.8	100.4
Fs	46.8	49.1	51.5	47.1	44.3	42.3	44.9
Wo	16.6	13.3	11.2	16.0	19.8	9.1	9.1
Plagioclase							
Number of grains	32	8	8	8	8	8	10
SiO_2	46.4	45.8	46.6	46.2	46.0	45.2	45.3
Al_2O_3	33.9	34.6	34.7	34.8	35.1	35.6	35.0
FeO	0.18	n.d.	n.d.	n.d.	n.d.	n.d.	n.d.
CaO	17.9	18.2	18.3	18.3	18.3	18.6	18.5
Na_2O	1.1	0.94	0.99	0.98	1.0	0.72	0.79
K_2O	0.08	0.06	0.08	0.08	0.08	0.07	0.07
Total	99.6	99.6	100.7	100.4	100.5	100.2	99.7
Ab	10.0	8.5	8.9	8.8	8.9	6.5	7.2
Or	0.5	0.4	0.5	0.5	0.5	0.4	0.4
Silica							
Number of grains	8			2		1	
SiO_2	99.4			99.6		101.1	
Al_2O_3	0.27			0.20		0.06	
FeO	0.26			n.d.		n.d.	
CaO	0.10			0.06		0.10	
Na_2O	< 0.02			< 0.02		< 0.02	
K_2O	0.14			0.14		< 0.02	
Total	100.2			100.0		101.3	

n.d. = not determined.

interstitial pyroxene forming an orthocumulate texture. The diverse textures within pebble 1 suggest that this rock may be a polymict breccia. Subsequent moderate annealing is probably responsible for the lack of observable clast boundaries.

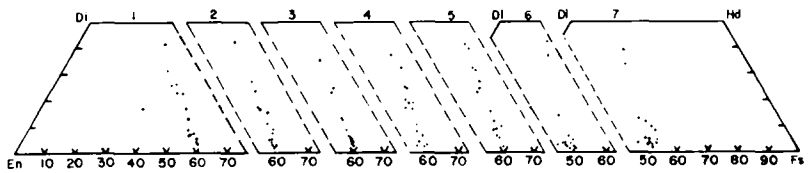

Fig. 1. Distributions of pyroxene compositions in the Vaca Muerta pebbles. Linear trends result from electron beam overlap on orthopyroxene and on augite exsolution lamellae. Pyroxene in pebbles 1–4 is more ferroan than in pebbles 6 and 7. One grain in pebble 1 lies off the trend, consistent with petrographic evidence that pebble 1 is an incompletely equilibrated polymict breccia.

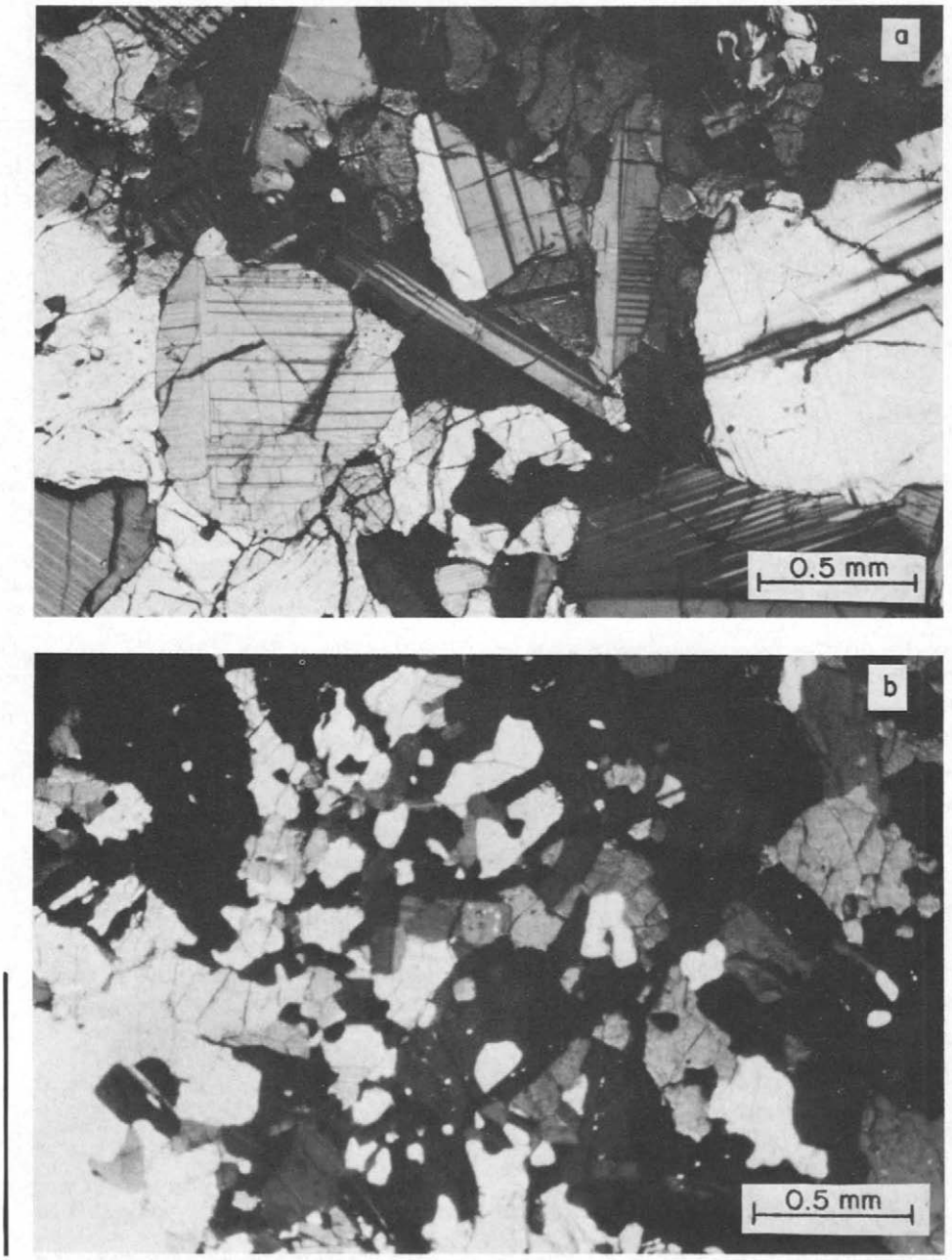

Fig. 2. (a) Predominant subophitic texture of pebble 1 consisting of twinned laths of plagioclase partially surrounding grains of inverted pigeonite. (b) Fine-grained region of pebble 1. The apparent absence of clast boundaries in the pebble is probably due to annealing. (a) and (b) in X-nicols.

Pebble 2 contains 1- to 6-mm angular to irregular clumps of anhedral to rounded, randomly-oriented, pyroxene grains embedded in a matrix of fine-grained (15–25 μm) plagioclase and trace amounts of pyroxene. The matrix is poorly crystallized and appears to be a devitrified plagioclase-rich glass (Fig. 3). Also present are individual $\leqslant 1$ mm grains of pyroxene and plagioclase and rare ($\sim 3 \times 7$ mm) subophitic clasts (Fig. 3). Crystal boundaries throughout the pebble are poorly de-

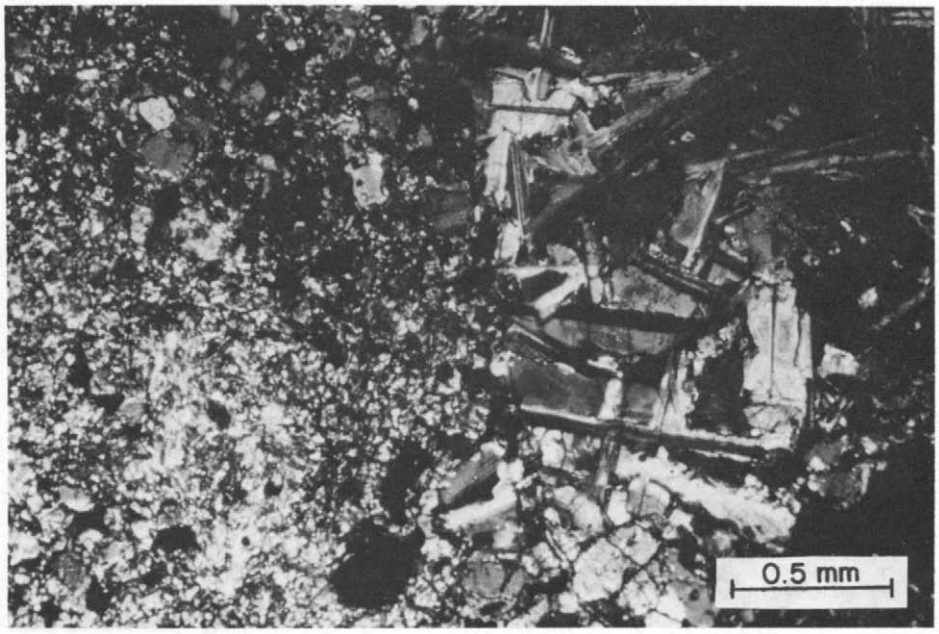

Fig. 3. Subophitic clast (right) and poorly-crystallized patch of plagioclase (light area at center of SW quadrant) in pebble 2. Most of the plagioclase has been remelted, suggesting that pebble 2 is an impact melt-breccia. The subophitic clasts may represent relict parental material. X-nicols.

fined and it appears that the pebble has been annealed. Because most plagioclase occurs as a devitrified glass, it seems likely that pebble 2 has been remelted and is an impact-melt breccia; the rare subophitic clasts may represent relict, unmelted portions of the original rock.

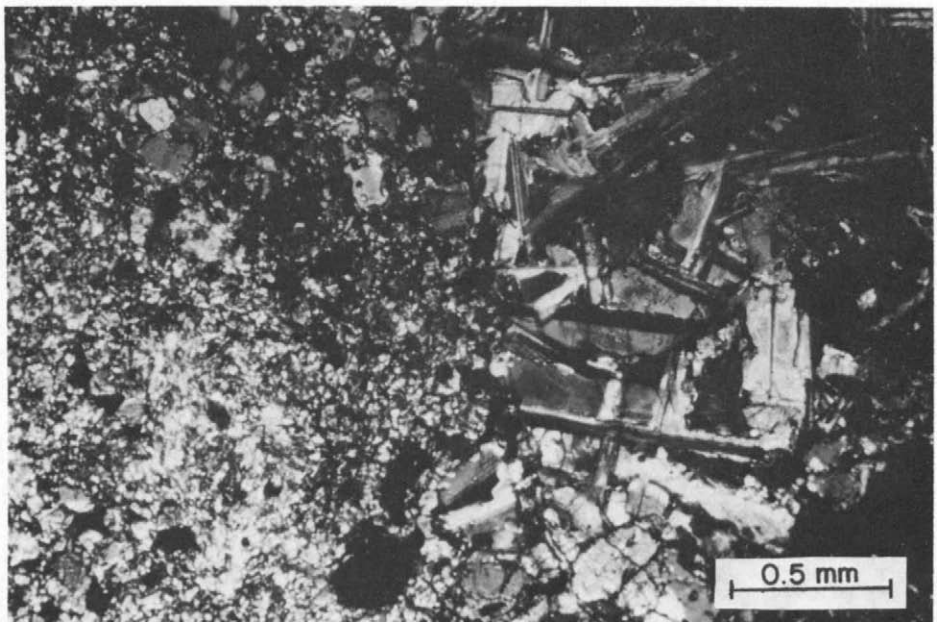

Fig. 4. Hypidiomorphic equigranular texture in pebble 3 consisting predominantly of plagioclase (light gray) and inverted pigeonite (dark gray). The pebble appears unbrecciated. Transmitted light.

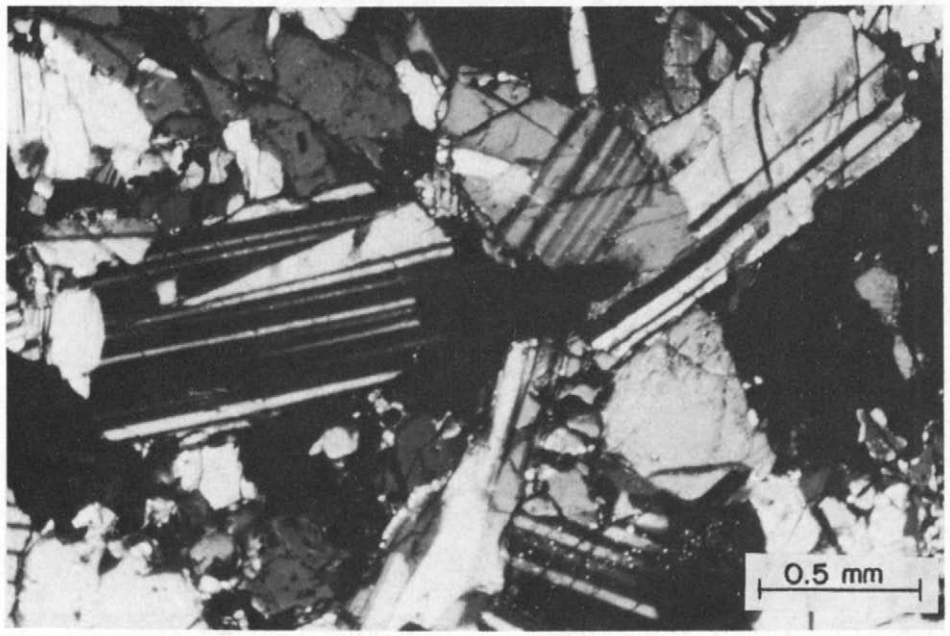

Fig. 5. Tabular, polysynthetically-twinned plagioclase grains and interstitial anhedral pyroxene in pebble 4 forming an orthocumulate texture. X-nicols.

Pebble 3 appears unbrecciated. It has a fine-grained (~ 100 μm) hypidiomorphic equigranular texture (Fig. 4).

Pebble 4 is a plagioclase orthocumulate containing tabular ~ 800 μm plagioclase grains and intercumulus pyroxene (Fig. 5). One centimeter-size area has a much higher plagioclase/pyroxene ratio than other areas and is texturally a mesocumulate. The orthocumulate areas resemble some regions of pebble 1.

Pebble 5 is another impact-melt breccia. It contains alternating, preferentially-oriented ~ 0.5 × 3 mm bands of pyroxene-rich clumps and matrix (Fig. 6a). The matrix is composed of small (25–100 μm), well-crystallized plagioclase grains with 120° triple junctures (Fig. 6b). Individual pyroxene and plagioclase grains in the bands of pebble 5 are oriented randomly relative to adjacent grains. Opaque phases occur predominantly inside the pyroxene-rich clumps.

Pebble 6 is an unbrecciated equigranular cumulate with an average grain size of 1200 μm (Fig. 7). Many plagioclase-plagioclase and plagioclase-pyroxene contacts form 120° triple junctures. Pebbles 8 and 10 are texturally very similar to pebble 6 and have respective average grain sizes of 850 μm and 1400 μm, respectively. One plagioclase grain in pebble 10 is 1700 × 4000 μm in size.

Pebble 7 is a fragmental breccia containing large (800–1400 μm) isolated subhedral and anhedral grains of plagioclase and pyroxene and 5 mm polymineralic basaltic clasts with hypidiomorphic-granular textures. The mineral grains and lithic clasts are embedded in a fine-grained (25–50 μm) matrix (Fig. 8) that consists of annealed pyroxene, plagioclase and silica, and has an allotriomorphic-granular texture. Opaque phases are heterogeneously distributed, being more abundant in the basaltic clasts than in the matrix.

Pebble 9 is an apparently unbrecciated plagioclase orthocumulate texturally similar to pebble 4. Tabular plagioclase grains (1000 μm) are surrounded by finer-grained intercumulus pyroxene. In some areas, plagioclase forms needles and the texture is subophitic. Almost all of the opaque grains occur inside pyroxene.

3.2. Bulk compositions

Bulk compositional data are listed in Table 1. Pebbles 1–4 have similar concentrations of incompatible elements; concentrations are lower in peb-

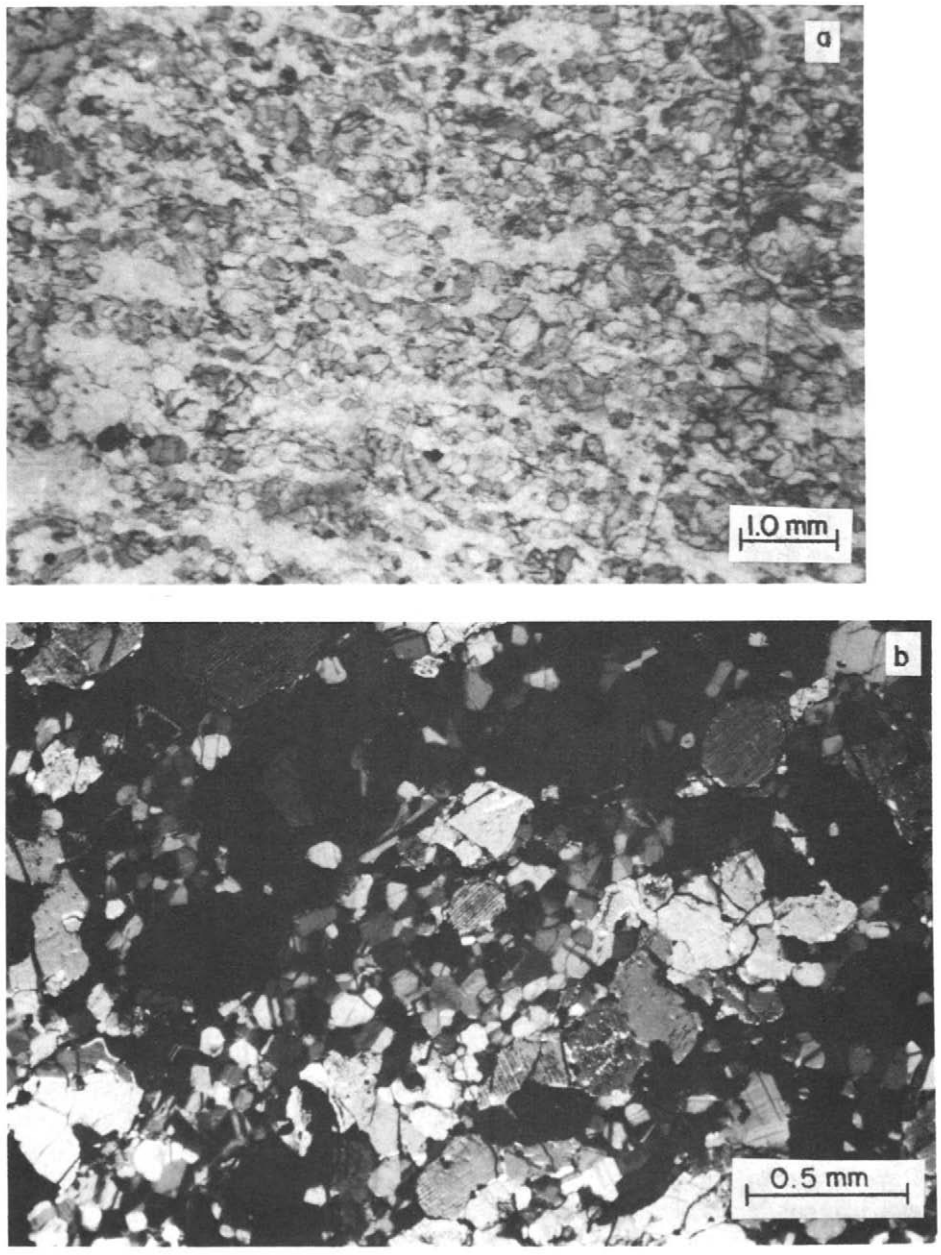

Fig. 6. (a) Alternating bands of plagioclase grains (light gray) and pyroxene (dark gray) preferentially oriented in a horizontal (E-W) direction in pebble 5. (b) Plagioclase band oriented NE-SW consisting of randomly oriented grains, many with 120° triple junctures. Pebble 5 is an impact-melt breccia; the texture indicates that the pebble experienced an episode of shock-melting and shearing. (a) in transmitted light; (b) in X-nicols.

ble 5 and very much lower in 6 and 7. The REE patterns (Fig. 9) in pebbles 1–4 are at 6–8 × H-chondrites and relatively flat, being only slightly depleted in light REE. They have small positive Eu anomalies. Of these four, pebble 2 has the highest REE concentrations and the smallest positive Eu anomaly; its normalized Eu/Sm ratio is only 1.12, whereas those of pebbles 1, 3 and 4 average 1.34. Pebble 5 differs from the others in having a fractionated REE pattern (with light

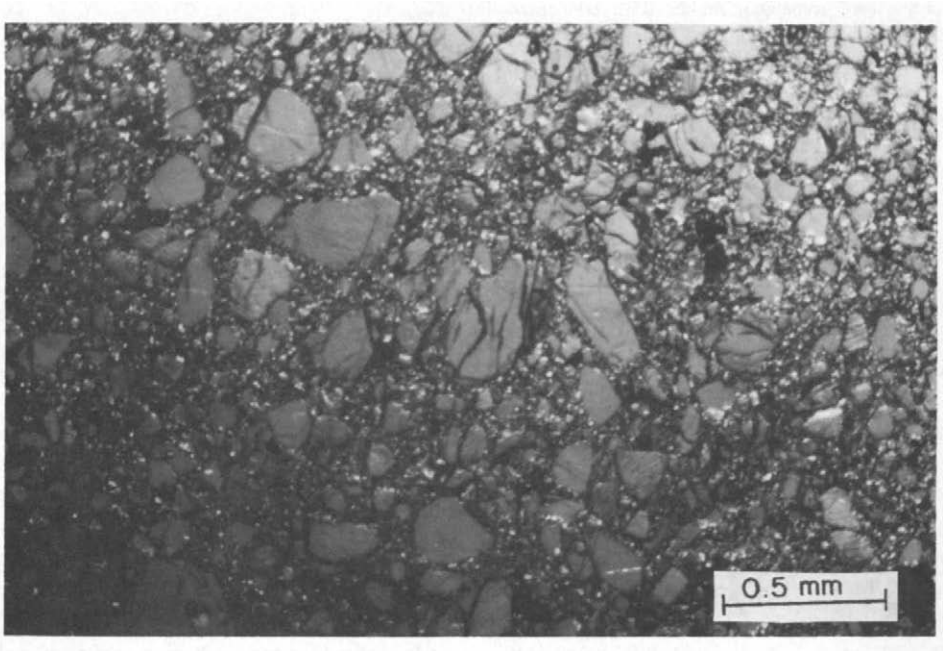

Fig. 7. Relatively coarse-grained cumulate texture of pebble 6. Several pyroxene grains exhibit simple twinning. One inverted pigeonite (bottom left) has a thick augite exsolution lamella parallel to (001). X-nicols.

REE 2 × depleted) at 2.2–5 × H with a significant positive Eu anomaly; its normalized Eu/Sm ratio is 2.53. Pebbles 6 and 7 have very low REE concentrations and extremely fractionated REE patterns; their normalized Eu/Sm ratios are 223 and 99.7, respectively. H-chondrite-normalized

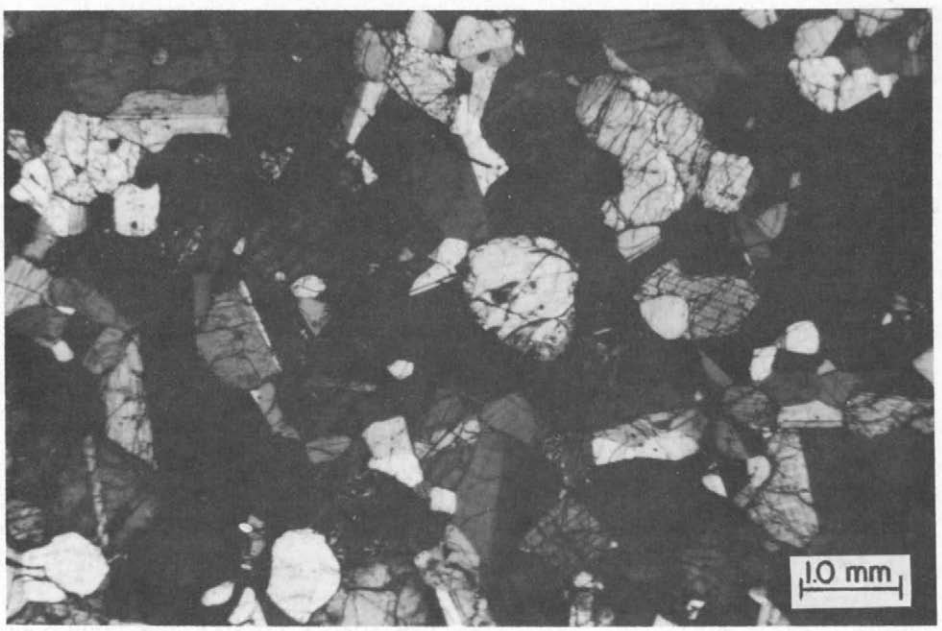

Fig. 8. Fragmental-brecciated texture of pebble 7 consisting of plagioclase and pyroxene grains and lithic clasts embedded in a fine-grained matrix. Transmitted light.

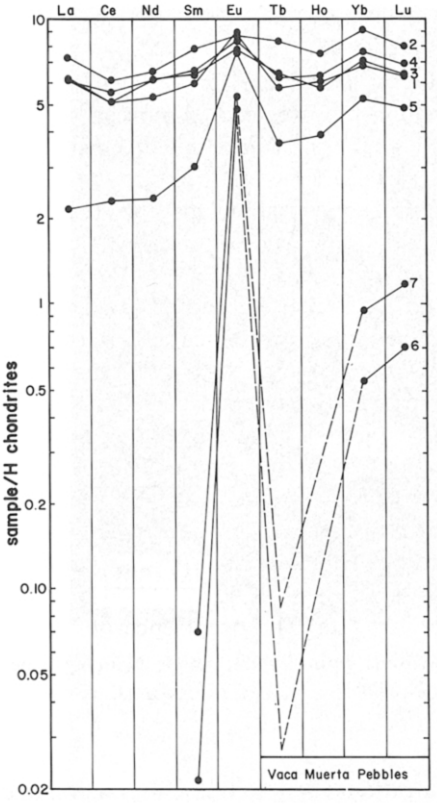

Fig. 9. H-chondrite-normalized concentrations of rare earth elements (REE) in the Vaca Muerta pebbles. Pebbles 1–4 have roughly flat REE patterns with small positive Eu anomalies; main-group eucrites have somewhat higher REE concentrations and slightly negative Eu anomalies. The REE pattern of pebble 5 is similar to that of cumulate eucrites. Pebbles 6 and 7 have extremely low REE concentrations, reflecting the virtual absence of intercumulus liquid. Very rough estimates of Tb concentrations in these two pebbles are also shown.

Ti/Al and Ti/Ca ratios are 1.04–1.62 in pebbles 2–4, ~ 0.90 in pebble 1, 0.62 in pebble 5 and only 0.10–0.18 in pebbles 6 and 7. In addition to their low abundances of incompatible elements, pebbles 5–7 are distinguished by lower bulk Fe and lower FeO.

The bulk molar MgO/(MgO + FeO) ratio (*mg**) of the samples was determined from analyses of the fused beads, assuming that all Fe is present as FeO. The *mg** of pebbles 1–5 has a narrow range (0.39–0.40), whereas the *mg** of pebbles 6 and 7 is significantly larger (0.51 and 0.46, respectively) (Table 1).

Siderophile/Ni concentration ratios (i.e., Ir/Ni, Co/Ni, Au/Ni, Ga/Ni) have interpebble variations of factors of 2–6. An obvious potential source of the siderophiles is mesosiderite metal. Wasson et al. [8] analyzed Ni, Ir and Ga in Vaca Muerta metal and Bild et al. [9] analyzed metal from 11 mesosiderites. We used Vaca Muerta metal Ir/Ni and Ga/Ni [8] and mean mesosiderite metal Co/Ni and Au/Ni [9] to compare with the corresponding ratios of the Vaca Muerta pebbles: Co/Ni and Au/Ni ratios in the pebbles are within 15% of those of mesosiderite metal; however, Ga/Ni ratios are high by factors of ~ 20 and Ir/Ni ratios are low by factors of ~ 10. Gallium concentrations in the pebbles are similar to those of eucrites (1–2 μg/g); the high Ga/Ni ratio indicates that the Ga is largely lithophile. The low Ir/Ni ratio cannot be due to lithophilic Ni; pigeonite and plagioclase in the Haraiya eucrite have very low Ni concentrations (20 and < 20 μg/g, respectively; [10]). Thus, the only major discrepancy between siderophiles in the pebbles and in mesosiderite metal is the low Ir of the former. Although Fukuoka et al. [11] recognized a chondritic component in the siderophiles of howardites, it is unlikely that the metal in the pebbles is chondritic: fine-grained metal in the Jilin H5 chondrite [12] has a higher Ir/Ni ratio.

4. Discussion

4.1. Similarity to basaltic achondrites

Although all of the Vaca Muerta pebbles are basaltic, they differ from known eucrites in their higher abundances of merrillite and silica. Pebbles 1–4 resemble main-group eucrites in their modal abundances and compositions of pyroxene and plagioclase and in *mg**, but differ in having lower abundances of REE and positive Eu anomalies. Although pebble 1 resembles main-group eucrites in having a predominantly subophitic texture (Fig. 2a), the diversity of textures, variations in mineral proportions, and the occurrence of a pyroxene grain of aberrant composition (Fig. 1) suggest that pebble 1 is polymict. The orthocumulate textures of pebbles 4 and 9 (Fig. 5) also differ from main-group eucrite textures. The hypidiomorphic equigranular texture of pebble 3 (Fig. 4) is most similar to that of Emmaville [13]. Pebble 2 is an impact-melt breccia, wherein almost all of the plagioclase occurs in a poorly-crystallized matrix (Fig. 3). This texture is not known among eucrites.

Perhaps most similar is Cachari, which contains glassy shock veins, in which quench-textured pyroxene occurs inside feldspathic glass [14, fig. 2].

Pebble 5 resembles main-group eucrites in having significantly more modal pyroxene than plagioclase, similar compositions of pyroxene and plagioclase and similar mg^* (~ 0.40), but resembles cumulate eucrites in its low REE abundances ($< 6 \times$ H) and in having a significant positive Eu anomaly. Light REE are more depleted than in cumulate eucrites. Bulk concentrations of Ti and FeO are intermediate between main-group and cumulate eucrites. A major difference between pebble 5 and known eucrites is its unusual impact-melt-breccia texture consisting of alternating bands of pyroxene and plagioclase (Fig. 6a, b).

Pebbles 6, 8 and 10 are unbrecciated and have equigranular cumulate textures (e.g., Fig. 7), resembling those of Moore County [15] and Moama [16]. The relatively refractory pyroxene and plagioclase, low bulk concentrations of incompatible elements and high mg^* in pebble 6 also are similar to cumulate eucrites; the pebble's bulk FeO/MnO ratio (30.7) is close to that of Moama (29.7; [16]). Pebble 6 differs from cumulate eucrites primarily in its extremely low concentrations of REE and very high Eu/Sm ratio.

The fragmental texture of pebble 7 (Fig. 8) is almost identical to that of the Bununu howardite [17, fig. 8.5a]. However, the apparent absence of a diogenite component [Fs (0–30) orthopyroxene] indicates that the pebble is a polymict eucrite (by the definition of [18]). Although some howardites and polymict eucrites contain impact-melt-rock clasts, crystalline chondrule-like spherules and CM-chondrite-like clasts, such objects were not found in pebble 7. Pyroxene and plagioclase abundances are similar to those of main-group eucrites; however, pyroxene and plagioclase compositions, bulk FeO/MnO (32.8) and mg^* (0.46) are more similar to cumulate eucrites.

In summary, there are significant differences between the Vaca Muerta pebbles and basaltic achondrites, including the unusual impact-melt breccia textures of pebbles 2 and 5, the excessive silica and merrillite in all of the pebbles, the somewhat lower REE abundances and positive Eu anomalies of pebbles 1–4 relative to those of main-group eucrites, and the very low REE abundances and high H-chondrite-normalized Eu/Sm ratios of pebbles 6 and 7 relative to cumulate eucrites.

Pebbles 2 and 5 are impact-melt breccias and may well have possessed common eucritic textures prior to being shocked. The orthocumulate textures of pebbles 4 and 9 (Fig. 5) are not common to monomict eucrites, but may be similar to some of the numerous texturally diverse clasts that occur in polymict eucrites [18].

Mittlefehldt et al. [19] noted that mesosiderites have higher normative silica and phosphate than howardites and suggested that this may have been caused in part by reduction of FeO in olivine by P from mesosiderite metal resulting in the formation of metallic Fe, pyroxene and silica. Alternatively, the ferrosilite component of the pyroxene may have been reduced to produce metallic Fe, silica and free oxygen. Concomitant oxidation of the P reducing agent may be responsible for the formation of merrillite. The occurrence of many grains of merrillite and silica adjacent to grains of metallic Fe-Ni and troilite in the pebbles is consistent with these models.

4.2. Petrogenesis

It is useful to plot eucrite compositions on diagrams of incompatible element concentration vs. mg^* (Fig. 10). On such diagrams, two branches protrude from the main-group cluster. One is the Stannern trend, thought to represent eucrites formed by partial melting (e.g., [20,21]). The other is the Nuevo Laredo trend, representing eucrites derived by fractional crystallization. The main-group cluster itself may simply be the intersection of these two trends. Cumulate eucrites formed by the accumulation of phenocrysts at the periphery of a magma chamber; their Mg-rich compositions reflect parental liquids with much lower mg^* [22].

Pebbles 1–4 plot near the main-group eucrites; the similar compositions of these pebbles suggest that they all may have formed from the same parental magma. The REE pattern of pebble 5 (Fig. 9) is similar to that of cumulate eucrites, indicating that this pebble formed, at least in part, from cumulate material. This is consistent with the lower abundances of incompatible elements in pebble 5.

Like cumulate eucrites, pebble 6 must have formed by crystal accumulation from a liquid with significantly lower mg^* than that parental to

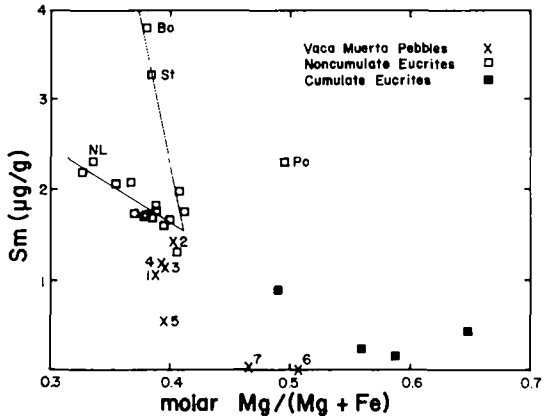

Fig. 10. Bulk composition of eucrites and Vaca Muerta pebbles expressed as Sm (μg/g) vs. molar MgO/(MgO+FeO) or *mg**. The cluster of points defines main-group eucrites; cumulate eucrites have high *mg** and low concentrations of incompatible elements. Two major compositional trends, the Nuevo Laredo (NL) and Stannern (St) trends are shown. Bouvante (Bo) lies along the Stannern trend; Pomozdino (Po) has an unusual composition and does not plot among the other eucrites. Pebbles 1–4 plot just below most main-group eucrites; pebble 5, with a lower Sm concentration, plots even lower. Pebbles 6 and 7, with high *mg** and extremely low concentrations of incompatible elements, plot near the cumulate eucrites.

main-group eucrites or pebbles 1–4. The extremely low concentrations of incompatible elements (typified by Sm) indicate that the residual liquid content of the pebble's parental material was very low, probably $\leqslant 1\%$. The Eu concentration in pebble 6 is $\sim 40\%$ lower than those in pebbles 1–5, but Sm is more than a hundredfold lower. The high Eu/Sm ratio in pebble 6 reflects the presence of pyroxene and plagioclase and the virtual absence of intercumulus liquid. Because pebbles 6 and 7 are similar in composition, both must have been derived from such liquid-poor cumulate material. Subsequent brecciation altered the original texture of pebble 7.

Individual plagioclase and pyroxene grains in the progenitors of pebbles 2 and 5 were partly melted and subjected to a (shock-induced) shearing stress, producing alternating pyroxene-rich and plagioclase-rich bands (much more pronounced in pebble 5 than in pebble 2). Random nucleation and growth of grains occurred in the sheared crystals, producing randomly oriented grains in the bands.

The low Ir/Ni ratios in the pebbles (relative to that of mesosideritic or chondritic metal) may also have resulted from shock processes. Widom et al. [12] found that metal nodules in ordinary chondrites are depleted in Ir and refractory siderophiles other than W by large factors relative to typical fine-grained matrix metal; they proposed that shock-induced vaporization of chondritic material was responsible. It seems possible that analogous processes in the Vaca Muerta regolith (i.e., shock-induced vaporization of mesosideritic material) are responsible for the low Ir/Ni ratios of the pebbles.

The occurrence of plagioclase with 120° triple junctures and the uniformity of mineral compositions indicate that the pebbles have been equilibrated. Because all of the pebbles are at least partly equilibrated and all seem to have reacted with metal, we favor pebble annealing after formation of the Vaca Muerta metal-silicate assemblage.

4.3. Impact gardening

The diverse textures of the pebbles indicate that they formed at a variety of depths. Impact processes are probably responsible for excavating the more deeply-buried rocks (e.g., pebble 10) and mixing them with rocks that formed closer to the surface (e.g., pebble 3). The shapes of the pebbles (angular to subrounded) reflect variable abrasion in the regolith.

After the pebbles had been mixed with metal and incorporated into the Vaca Muerta host, a period of heating caused reaction of the pebbles with the metal: FeO in the silicates was reduced, some P from the metal was oxidized, and merrillite and excess silica were formed in the pebbles. Impacts probably were the dominant heat source responsible for this annealing [23].

A high impact rate at the surface of the basaltic achondrite parent body is consistent with the brecciated nature of mesosiderites, howardites and non-cumulate eucrites. However, it appears that mesosiderites experienced more extensive heating than either howardites or eucrites. Although howardites contain a few impact-melt-rock clasts and crystalline chondrule-like spherules, howardites contain few, if any, pebble-size impact-melt breccias. The Cachari eucrite contains shock veins, but most areas of Cachari have not been impact-

melted. In contrast, type 4 mesosiderites, which constitute ~ 35–40% of known mesosiderites [3, table 1] appear to have been entirely impact-melted [2,3,24]. Two of the 10 Vaca Muerta pebbles (20%) also appear to have been impact-melted.

We suggest three alternative models to explain the greater proportion of impact-melted material among mesosiderites:

(1) Mesosiderites were derived from a different parent body than eucrites, howardites and diogenites with the mesosiderite parent body experiencing a higher meteoroid fluence.

(2) Mesosiderites are from the same parent body as the basaltic achondrites, but mesosideritic regolith experienced more extensive impact-melting than other regions, perhaps because the accretion of large metallic core fragments from disrupted differentiated asteroids onto these regions resulted in more extensive heating (and heat retention) in mesosiderites. Wasson and Rubin [25] suggested that such core fragments accreted to the regolith of a basaltic achondrite parent body at low relative velocities (~ 1 km s^{-1}). Such low velocities can only cause melting (e.g., [26, fig. 2]) if the heat is efficiently trapped and distributed nonuniformly. The accretion of core fragments may have provided both extensive heating of the regolith and the coarse (metallic) particles necessary for significant heat retention.

(3) Portions of all regolithic regions suffered extensive shock-heating. Metal-free howarditic regions tended to be ground mechanically into finer particles that cooled quickly by radiation. In the case of the mesosiderites, the abundant coarse metal allowed significant heat retention and welding of regolith material into larger and tougher objects better able to survive the rigors of interplanetary space. We favor the second and third alternative models.

Acknowledgements

We thank J.T. Wasson, R.H. Hewins and P.H. Warren for numerous constructive comments, F. Begemann, R. Hutchison and an anonymous referee for useful reviews, and R.E. Jones, G.W. Kallemeyn, L. Mikami, A. Pang, H. Qian and D.N. Shirley for technical assistance. We are especially grateful to R. Haag for supplying the Vaca Muerta specimens. This work was mainly supported by National Aeronautics and Space Administration grant NAG 9-40.

References

1 B.N. Powell, Petrology and chemistry of mesosiderites, II. silicate textures and compositions and metal-silicate relationships, Geochim. Cosmochim. Acta 35, 5–34, 1971.
2 R.J. Floran, Silicate petrography, classification, and origin of the mesosiderites: Review and new observations, Proc. 9th Lunar Planet. Sci. Conf., pp. 1053–1081, 1978.
3 R.H. Hewins, The case for a melt matrix in plagioclase-POIK mesosiderites, Proc. 15th Lunar Planet. Sci. Conf., J. Geophys. Res. Suppl. 89, C289–C297, 1984.
4 A.E. Bence and A.L. Albee, Empirical correction factors for the electron microanalysis of silicates and oxides. J. Geol. 76, 382–404, 1968.
5 P.A. Baedecker, SPECTRA: computer reduction of gamma-ray spectroscopic data for neutron activation analysis, in: Advances in Obsidian Glass Studies: Archeological and Geochemical Perspectives, R.E. Taylor, ed., pp. 344–349, Noyes Press, 1976.
6 J.N. Grossman and P.A. Baedecker, Computer graphics for quality control in the INAA of geological samples, Proc. 7th Int. Conf. on Modern Trends in Activation Analysis, pp. 571–578, 1986.
7 G.E. Harlow and R. Klimentidis, Clouding of pyroxene and plagioclase in eucrites: implications for post-crystallization processing, Proc. 11th Lunar Planet. Sci. Conf., pp. 1131–1143, 1980.
8 J.T. Wasson, R. Schaudy, R.W. Bild and C.-L. Chou, Mesosiderites, I. Compositions of their metallic portions and possible relationship to other metal-rich meteorite groups, Geochim. Cosmochim. Acta 38, 135–149, 1974.
9 R.W. Bild, K.L. Robinson, E.R.D. Scott and M. Prinz, Origins of mesosiderites as inferred from instrumental neutron activation analysis of their metallic Fe,Ni (abstract), Meteoritics 18, 266–267, 1983.
10 B. Mason and A.L. Graham, Minor and trace elements in meteoritic minerals, Smithsonian Contrib. Earth Sci. 3, 1–17, 1970.
11 T. Fukuoka, W.V. Boynton, M.-S. Ma and R.A. Schmitt, Genesis of howardites, diogenites and eucrites, Proc. 8th Lunar Sci. Conf., pp. 187–210, 1977.
12 E. Widom, A.E. Rubin and J.T. Wasson, Composition and formation of metal nodules and veins in ordinary chondrites, Geochim. Cosmochim. Acta 50, 1989–1995, 1986.
13 B. Mason, E. Jarosewich and J.A. Nelen, The pyroxene-plagioclase achondrites, Smithsonian Contrib. Earth Sci. 22, 27–45, 1979.
14 D.D. Bogard, G.J. Taylor, K. Keil, M.R. Smith and R.A. Schmitt, Impact melting of the Cachari eucrite 3.0 Gy ago, Geochim. Cosmochim. Acta 49, 941–946, 1985.
15 H.H. Hess and E.P. Henderson, The Moore County meteorite: a further study with comment on its primordial environment, Am. Mineral. 34, 494–507, 1949.
16 J.F. Lovering, The Moama eucrite—a pyroxene-plagioclase adcumulate, Meteoritics 10, 101–114, 1975.

17 R.T. Dodd, Meteorites—A Petrologic-Chemical Synthesis, Cambridge, 368 pp., 1981.
18 J.S. Delaney, M. Prinz and H. Takeda, The polymict eucrites, Proc. 15th Lunar Planet. Sci. Conf., pp. C251–C288, 1984.
19 D.W. Mittlefehldt, C.-L. Chou and J.T. Wasson, Mesosiderites and howardites: igneous formation and possible genetic relationships, Geochim. Cosmochim. Acta 43, 673–688, 1979.
20 G.J. Consolmagno and M.J. Drake, Composition of the eucrite parent body: evidence from rare earth elements, Geochim. Cosmochim. Acta 41, 1271–1282, 1977.
21 Basaltic Volcanism Study Project, Basaltic Volcanism on the Terrestrial Planets, 1286 pp., Pergamon Press, New York, N.Y., 1981.
22 E. Stolper, Experimental petrology of eucritic meteorites, Geochim. Cosmochim. Acta 41, 587–611, 1977.
23 L.E. Nyquist, H. Takeda, B.M. Bansal, C.-Y. Shih, H. Wiesmann and J.L. Wooden, Rb-Sr and Sm-Nd internal isochron ages of a subophitic basalt clast and a matrix sample from the Y75011 eucrite, J. Geophys. Res. 91, 8137–8150, 1986.
24 R.H. Hewins and T.A. Harriott, Melt segregation in plagioclase-poikilitic mesosiderites, Proc. 16th Lunar Planet. Sci. Conf., pp. D365–D372, 1986.
25 J.T. Wasson and A.E. Rubin, Formation of mesosiderites by low-velocity impacts as a natural consequence of planet formation, Nature 318, 168–170, 1985.
26 F. Hörz and R.B. Schaal, Asteroidal agglutinate formation and implications for asteroidal surfaces, Icarus 46, 337–353, 1981.